Research article

An application of mobile robotics for olfactory monitoring of hazardous industrial sites

Cosimo Distante
Institute for Microelectronics and Microsystems IMM-CNR, Lecce, Italy, and

Giovanni Indiveri and Giulio Reina
Department of Innovation Engineering, University of Salento, Lecce, Italy

Abstract

Purpose – The purpose of this paper is to present a mobile robot with an olfactory capability for hazardous site survey. Possible applications include detection of gas leaks and dangerous substances along predefined paths, inspection of pipes in factories, and mine sweeping.

Design/methodology/approach – The mobile sentry is equipped with a transducer array of tin oxide chemical sensors, compliant with the standard interface IEEE 1451, which provides odour-sensing capability, and uses differential drive and spring-suspended odometric trackballs to move and localize in the environment. The monitoring strategy comprises two stages. First, a path learning operation is performed where the vehicle is remotely controlled through some potential critical locations of the environment, such as valves, pressure vessels, and pipelines. Then, the robot automatically tracks the prerecorded trajectory, while serving as an electronic watch by providing a real-time olfactory map of the environment. Laboratory experiments are described to validate the approach and assess the performance of the proposed system.

Findings – The approach was shown to be effective in experimental trials where the robot was able to detect multiple odour sources and differentiate between sources very close to one another.

Research limitations/implications – One limitation of the methodology is that it has been specifically designed for odour detection along a well-defined path in a highly structured environment, such as that expected in the industrial field. The problem of detection of leakages outside the search path is not addressed here.

Practical implications – This mobile robot can be of great value to detect hazardous fluid leakages in chemical warehouses and industrial sites, thus increasing the safety level for human operators.

Originality/value – The paper describes a mobile robotic system, which employs an odour-sensing capability to perform automated monitoring of hazardous industrial sites. A dynamic model of the mobile nose is also discussed and it is shown that it well describes the behaviour of the system.

Keywords Robotics, Intelligent sensors, Hazardous materials, Chemical hazards, Condition monitoring

Paper type Research paper

1. Introduction

One of the greatest challenges among the robotics research community is the development of intelligent vehicles capable of autonomous navigation in structured and unstructured environments. Such vehicles will rely on complex sensing systems, able to gather the relevant features of the environment, and intelligent control systems that produce the appropriate actions in response to the sensed surroundings. Since, when Persaud and Dodd (1982) described in their seminal paper a model of an artificial system able to emulate some aspects of the biological olfactory system and now commonly known as an "electronic nose," a great deal of interest arouse in the robotics community. A significant example of an electronic nose – ENose, was developed by JPL for detecting chemical leaks in enclosed spaces, like the International Space Station or Space Shuttle (Ryan *et al.*, 2004). Recently, in the MIR space station an array of conductive polymer sensors where used to detect fluid leak of ethylene glycol in the cooling system (Persaud *et al.*, 1999). Gas sensors have been widely used in food analysis (Taurino *et al.*, 2003), such as tests on the freshness of fish (Olafsson *et al.*, 1992), quality estimation of ground meat (Winquist *et al.*, 1993), and recognition of illegally produced spirituous beverages (Kleperis *et al.*, 1999). Although it is rather common to find robots with sensors that mimic the animal world, sensors for smell (chemical sensors) are by far the least used in robotics. The reason relies not only in the reduced importance of this sense in human navigation, but also a consequence of the slow development of chemical sensors in

The current issue and full text archive of this journal is available at **www.emeraldinsight.com/0143-991X.htm**

Industrial Robot: An International Journal
36/1 (2009) 51–59
© Emerald Group Publishing Limited [ISSN 0143-991X]
[DOI 10.1108/01439910910924675]

The authors would like to thank Giovanni Sammarco who conducted many of the experiments described in this paper during his Master's Diploma Thesis work.

Industrial Robot: An International Journal
Volume 36 · Number 1 · 2009 · 51–59

order to become similar to their biological counterparts (Russell, 2001).

A mobile robot can take advantage of an electronic nose when it needs to perform some chemically related tasks, such as identification of washed areas by cleaning robots, follow an odour track or find sources of odour, like gas leaks, drugs, explosives, and landmines. Many research groups have addressed the implementation of odour sensors in the robotics field. Russell *et al.* (1995) at Monash University in Australia described an interesting approach in navigation of mobile robots, based on laying down an odour trail and using an olfactory sensor to allow a vehicle to follow the trail or to guide other following robots. Marques and de Almeida (2000) developed insect behaviour-based algorithms in order to follow the chemical gradient of an odour plume rather than a trail. The insect world demonstrates that the laying and detection of chemical trails can be useful as an aid for navigation and to help organise large groups of workers. With similar navigation and organisational benefits in mind, robotic trail following has also been investigated in Stella *et al.* (1995). The localization of odour sources was also demonstrated in special environments: constant airflow and the use of huge sources with special odours. The constant airflow results in enormous advantage in locating gas sources, since the gas source generates a plume, with a well-defined concentration profile stable in time. In all those cases, an upwind search can be performed by driving across the plume (Nakamoto *et al.*, 1999; Ishida *et al.*, 1994). The foremost limitation of odour-based navigation is the vehicle slow speed (<20 cm/s). In the last few years, there has been an increasing demand for gas sensors to inspect chemical warehouses and industrial sites against leakages of hazardous chemicals.

This paper describes the efforts at the University of Salento towards the development of a mobile "sentry" with olfactory capability for intelligent monitoring of the environment. A differential drive mobile robot is equipped with a gas sensor device developed at the Institute for Microelectronics and Microsystems of the University of Lecce in Italy. It consists of an array of four tin oxide sensors enclosed in a ventilated cell and features IEEE Std. 1451.2 (1997) interface, which ensures plug and play (PnP) capability. The olfactory sensor enables the robot to build real time odour maps, and serves as a mobile electronic watch for automated monitoring of hazardous industrial sites. The designed strategy for environment inspection is performed in two stages. In the first step, the vehicle learns the inspection path driving by potential leaking locations of the environment in remote control mode. The second step is the automated olfactory inspection process aiming at detecting odour sources, which would indicate gas leaks along the prerecorded path. During the automated inspection stage, the robot is controlled by a non-linear feedback trajectory tracking law. A spline-based path generator is also presented that allows the mobile robot to return autonomously and smoothly to the starting spot, at the end of the path learning operation.

The paper is organized as follows. Section 2 describes the olfactory unit in detail. The mobile robot used as a test bed for experimental validation is presented in Section 3. Section 4 discusses the approach proposed for olfactory monitoring of the environment, whereas Section 5 describes a dynamic model of the mobile nose, and provides experimental results and comments. Finally, Section 5 concludes this paper.

2. The olfactory sensor

The olfactory unit, shown in Figure 1(a), detects gas mixtures using an array of tin oxide gas sensors manufactured by Microsens (MSGS 4000), and mounted within a nylon chamber so-called nose cap, which is shown in Figure 1(b). A pump is used for blowing odour-laden air into and out of the chamber with an airflow of $6\,m^3/h$, and for stirring the vapors. The nose cap allows the spatial differentiation of the mobile nose to be increased, and the change rate of air at the sensor's location to be improved. Thus, possible effects due to different driving speeds are reduced. The continuous air stream also allows for avoiding the degradation of the metal oxide sensors saturation level observed with very low-air movement relative to the sensor, and lower the time needed for the sensors to recover after the odour stimulus is removed (Lilienthal *et al.*, 2001). Tin oxide sensors are inexpensive, small in size, have relatively low-power consumption, and are relatively unaffected by changing environmental conditions like room temperature or humidity. However, they feature very low selectivity. Thus, although the sensitivity of the Microsens sensors used in this work is optimized for solvents, halocarbons, and a range of combustible gasses, they respond strongly to alcoholic substances, which were used to provide the gas source in our experiments. The transducer principle is based on heating the tin oxide sensor to about 300°C, where the presence of reducing gasses causes a drop in sensor resistance. The relationship between sensor resistance and the concentration of detected gas is nonlinear and can be approximated by (Watson, 1984):

$$R \cong K \cdot R_0 \cdot C^{\alpha}, \tag{1}$$

where α is the sensitivity, R is the sensor resistance, R_0 is the sensor resistance in clean air, K is the scaling constant, and C is the concentration. The resistance of tin oxide sensors increases as the concentration of the target chemical is reduced. This implies a negative value for the sensitivity constant α. When an odour is presented to the electronic nose, most if not all sensors will respond to same extent. However, some will respond far more strongly than others. Preprocessing typically involve normalization to account for variations in odour concentration.

The olfactory unit is compliant with IEEE 1451.2 standard. Specifically, a Smart Transducer Interface Module (STIM) has been developed providing PnP capabilities for the transducer at both hardware and software level. PnP is twofold operating at both local level, for adding/replacing new transducer devices, and network level in order to enable remote control/query from portable devices such as personal digital assistants, laptops, etc. The former is achieved with the definition of a transducer electronic data sheet (TEDS) that supports a wide variety of transducers. The TEDS, which provides self-identification capabilities, is the core of this sensorial device, since it contains fields that fully describe the type, operation, and attributes of one or more transducers. In general, IEEE 1451 is a family of standards, which introduces also an informative model of microprocessor named Network Capable Application Processor – NCAP (IEEE 1451.1), which is the bridge between the physical world of transducers and the network (regardless of the transport). This allows for PnP capability at network level, by managing a multitude of agents that interact to each other with the same communication language (Lee, 2000). The implementation

Figure 1 The olfactory sensor box (a), and a detail of the nose cap (b)

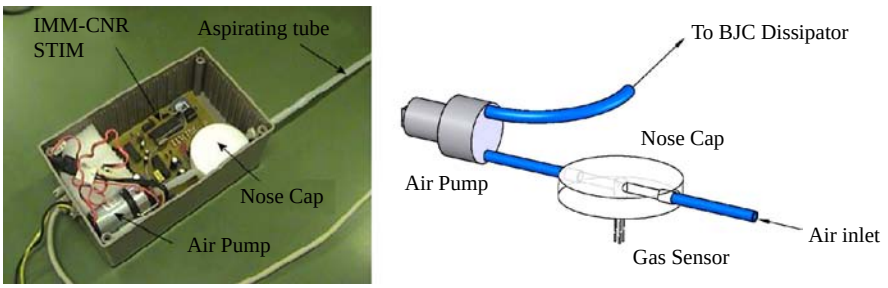

(a) (b)

of the IEEE 1451.2 standard is shown for the hardware and software part in Figure 2(a) and 2(b), respectively. In the reminder of this section, a brief description of each part is provided.

The STMicroelectronics ST72264G and the M24C64 EEPROM are the hardware base for the STIM. The ST72264G is an 8-bit Micro Controller Unit (MCU) with 8 KB of program memory, 256 Bytes of RAM, 22 multifunctional bidirectional I/O lines, an I2C multimaster interface, a SCI asynchronous serial interface and a 10-bit ADC with six input channels. Input to the MCU are the four semiconductor gas sensors and one temperature/humidity sensor. The M24C64 EEPROM is used to store the IEEE 1451.2 TEDS, while the data between EEPROM and MCU are transmitted via I2C interface.

The logical software block diagram of the STIM consists of five modules (Figure 2(b)):

1 *STIM control and channel data block.* Contains the definitions of the channels associated with the STIM and the main control flow.
2 *STIM-NCAP interface block.* Defines the logical interface between STIM and NCAP mapped on a RS232 link; asynchronous messages are defined for replacing trigger, acknowledgement, hot swap and error reporting functions, in addition to the data transfer functions.
3 *TEDS block.* Defines the TEDS that are in use in this implementation of the 1451.2. It defines where the TEDS are mapped to, how they are written, how they are retrieved and what they contain.
4 *Basic functions blocks.* Implements all the main functionalities that are defined by the 1451.2 standard. It deals with data transport, control, interrupt, status and trigger functions.
5 *STIM-transducer interface block.* Provides functions that allow to access to each channel of the STIM.

3. The mobile sentry Jack

All the experimental work described in this paper was performed using the mobile robot Jack, which is a differential drive vehicle built at the Applied Mechanics Laboratory of the University of Salento. The vehicle is shown in Figure 3(a), with the olfactory unit mounted on its top at a height of about 60 cm from the ground. Jack is equipped with a 1 GHz Pentium IV processor, and linked with the local network through a wireless connection. It can run in autonomous mode or be manually controlled using a wireless joypad. Its sensor suite includes various mechanical and infrared proximity sensors and a camera for off-board broadcasting. The vehicle can achieve speeds up to 1 m/s. It is special in the fact that it utilizes a position estimation system based on a pair of non-loading-bearing odometric two-axes trackballs rather than conventional encoders, mounted on the axes of the drive wheels. This solution is generally beneficial to odometric accuracy, since it results in a reduction of the typical systematic errors connected with slippage and deformability of loaded drive wheels (Borenstein and Feng, 1996). Each channel of the trackball has a resolution of

Figure 2 Block diagram of the STIM's hardware (a), and software part (b)

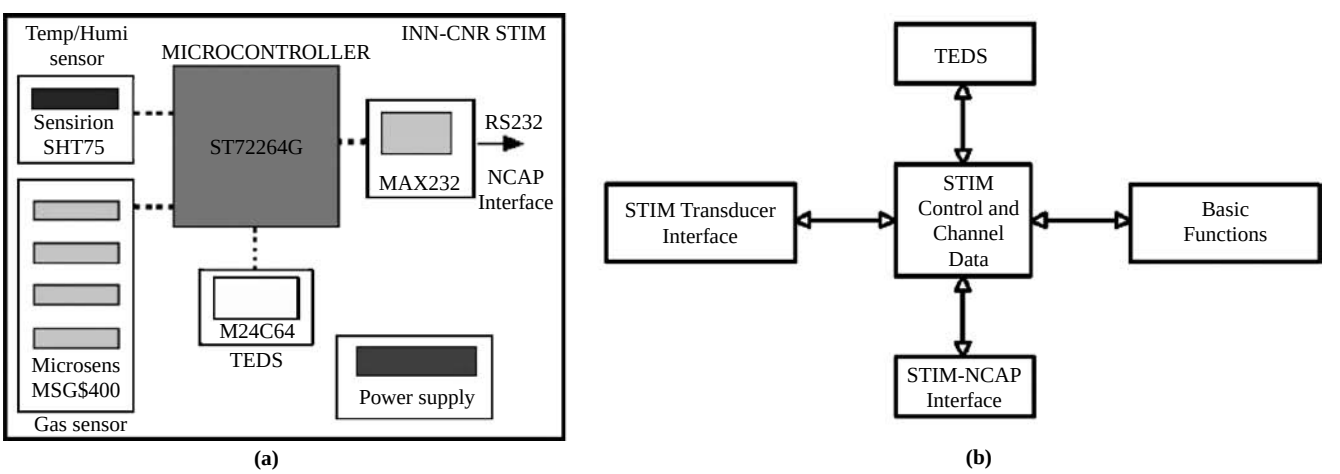

(a) (b)

Figure 3 The differential drive vehicle Jack (a), with a technical illustration of the trackball suspension system (b)

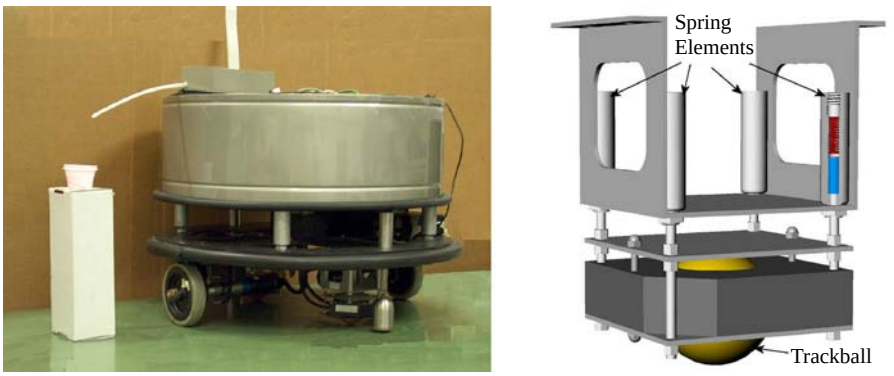

(a) **(b)**

960 lines/rev that implies for the 50.8 mm diameter of the trackball a sensitivity in terms of linear displacement of 0.16 mm. The two trackballs are suspended with a telescopic spring system, which enables the odometer to move up and down relative to the drive wheels, avoiding that small undulations in terrain can leave the vehicle supported only by the trackballs, while ensuring the required spring load with the pavement. Details of the telescopic suspension system and location of the trackballs are shown in Figures 3 and 4, respectively.

Figure 4 shows a schematic diagram of our vehicle Jack. A coordinate system is attached to the vehicle so that the x-axis of the vehicle coordinate system is aligned with the vehicle's longitudinal direction. The position of the vehicle traveling on a plane is fully described by the Cartesian coordinates X, Y and the heading θ (Yaw) of the midpoint G of the central axis, chosen as vehicle reference point. At the generic instant $t = nT$, the robot location update can be estimated as follows:

Figure 4 Pose estimation for the vehicle Jack

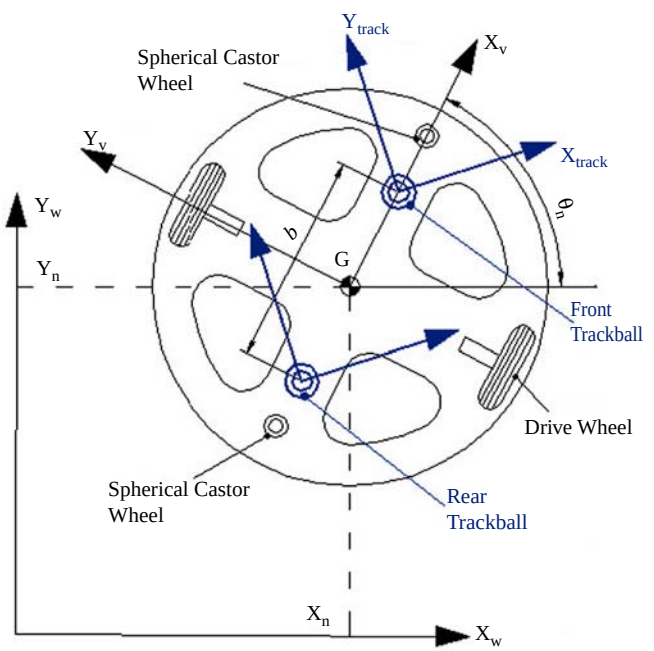

$$X_{n+1} = X_n + \delta d_n \cdot \cos\left(\theta_n + \frac{\delta\theta_n}{2}\right), \tag{2}$$

$$Y_{n+1} = Y_n + \delta d_n \cdot \sin\left(\theta_n + \frac{\delta\theta_n}{2}\right), \tag{3}$$

$$\theta_{n+1} = \theta_n + \delta\theta_n, \tag{4}$$

where δd_n and $\delta\theta_n$ are, respectively, the linear and angular displacement of the vehicle between two sampling points that can be estimated from the trackball pair as:

$$\delta\theta_n = \frac{\delta Y_{n,\mathrm{F}} - \delta Y_{n,\mathrm{R}}}{b}, \tag{5}$$

$$\delta d_n = \frac{\delta X_{n,\mathrm{F}} - \delta X_{n,\mathrm{R}}}{2}, \tag{6}$$

being b the distance between the trackballs along the vehicle longitudinal direction, and $\delta X_{n,i}$ $\delta Y_{n,i}$ the displacement measured by the trackball i (i = front, rear) along X_v- and Y_v-directions, respectively.

4. Olfactory monitoring

The strategy for the automated inspection of hazardous industrial environments comprises two stages. In the first stage, the vehicle records the path to be monitored while in remote control mode. A spline-based algorithm enables the vehicle to return to its starting spot at the end of this step. The second stage consists of the automated monitoring along the prerecorded path. This approach has been specifically designed for a structured environment with a high degree of automation and known critical hot spots for possible fluid or gas leakages, which is the typical case of industrial sites for production, storage and manipulation of hazardous products. In the reminder of this section, both stages of the olfactory monitoring are described in detail.

4.1 The path learning process

The mobile robot is remotely controlled by the operator through some critical locations of the environment $P = [P_1, P_2, \ldots, P_n]$ ($P_i \in R^2$ with respect to a given global frame, see Figure 5), via wireless communication using a joypad and an onboard camera, while it records the driven (manually commanded) path using its pose estimation system, as described in Section 3. This step is performed under the

Figure 5 The path learning process

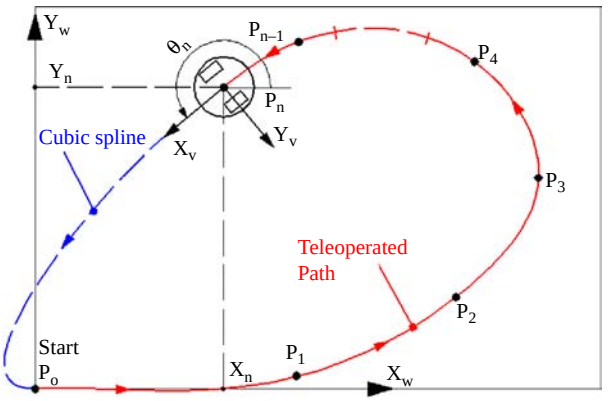

assumption that those locations are accessible by the robot and a clear route of connection can be done. During this stage, olfactory data are also stored to serve as a reference value for the successive inspection task. As shown in Figure 5, the recorded path might not be closed, i.e. the ending pose could differ from the starting one ($P_n \neq P_0$). Since in the next phase the robot should autonomously re-run the learned path to accomplish its environment monitoring task, poses P_0 and P_n need to be suitably connected. The issue is to find a path going from P_n to P_0 having, in P_n and P_0, the same slopes that the recorded one had. Moreover, in order to minimize the jerk, the curvature of the connecting path should be null in P_0 and P_n. These requirements call for a spline-based path planning approach.

In particular, if $\xi \in [0, 1]$ and $P_n = (x_n, y_n)$ and $P_0 = (x_0, y_0)$, a continuous curve going from P_n to P_0 with assigned derivatives in P_n and P_0 is given by:

$$\Gamma = \{(x(\xi), y(\xi)) : \xi \in [0, 1]\}, \tag{7}$$

where:

$$x(\xi) = a\xi^3 + b\xi^2 + c\xi + d, \tag{8}$$

$$y(\xi) = \alpha\xi^3 + \beta\xi^2 + \gamma\xi + \delta, \tag{9}$$

with the following boundary conditions:

$$x|_{\xi=0} = x_0 = d = x_{P_n}, \tag{10}$$

$$y|_{\xi=0} = y_0 = \delta = y_{P_n}, \tag{11}$$

$$x|_{\xi=1} = x_1 = a + b + c + d = 0, \tag{12}$$

$$y|_{\xi=1} = y_1 = \alpha + \beta + \gamma + \delta = 0, \tag{13}$$

$$\left.\frac{dy}{d\xi}\right|_{\xi=0} = y'|_{\xi=0} = y'_0, \tag{14}$$

$$\left.\frac{dy}{d\xi}\right|_{\xi=1} = y'|_{\xi=1} = y'_1, \tag{15}$$

$$\left.\frac{dx}{d\xi}\right|_{\xi=0} = x'|_{\xi=0} = x'_0, \tag{16}$$

$$\left.\frac{dx}{d\xi}\right|_{\xi=1} = x'|_{\xi=1} = x'_1, \tag{17}$$

The four derivatives x'_0, x'_1, y'_0, y'_1 are assumed to be known.

The slope of Γ at the two boundary points is:

$$\left.\frac{y'}{x'}\right|_{\xi=0} = \frac{y'_0}{x'_0} = \left.\frac{dy}{dx}\right|_{\xi=0}, \tag{18}$$

$$\left.\frac{y'}{x'}\right|_{\xi=1} = \frac{y'_1}{x'_1} = \left.\frac{dy}{dx}\right|_{\xi=1}, \tag{19}$$

while the curvature κ of the curve is given by:

$$\kappa = \frac{x'y'' - y'x''}{(x'2 + y'2)^{3/2}}, \tag{20}$$

In order for Γ to have null curvature in $\xi = 0$, $\xi = 1$, and contemporary satisfy the boundary conditions (10)-(17), it is sufficient to add to the relations (8) and (9) the polynomials $x_\kappa(\xi)$ and $y_\kappa(\xi)$, respectively, which satisfy the boundary conditions defined below:

$$x_\kappa(0) = x_\kappa(1) = 0, \tag{21}$$

$$x'_\kappa(0) = x'_\kappa(1) = 0, \tag{22}$$

$$x''_\kappa(0) = -x''(0) = -2b, \tag{23}$$

$$x''_\kappa(1) = -x''(1) = -6a - 2b, \tag{24}$$

and equivalently on $y_\kappa(\xi)$. By direct calculation, it can be found that such polynomials may be defined as:

$$x_\kappa(\xi) = (\xi(\xi - 1))^2(m_x\xi + q_x), \tag{25}$$

$$y_\kappa(\xi) = (\xi(\xi - 1))^2(m_y\xi + q_y), \tag{26}$$

where:

$$m_x = -3a, \quad q_x = -b, \tag{27}$$

$$m_y = -3\alpha, \quad q_y = -\beta, \tag{28}$$

Thus, the final expressions for $x(\xi)$ and $y(\xi)$ are:

$$x(\xi) = a\xi^3 + b\xi^2 + c\xi + d + (\xi(\xi - 1))^2(-3a\xi - b), \tag{29}$$

$$y(\xi) = \alpha\xi^3 + \beta\xi^2 + \gamma\xi + \delta + (\xi(\xi - 1))^2(-3\alpha\xi - \beta), \tag{30}$$

being:

$$a = -2(x_1 - x_0) + x'_0 + x'_1,$$

$$b = 3(x_1 - x_0) - 2x'_0 - x'_1,$$

$$c = x'_0,$$

$$d = x_0,$$

$$\alpha = -2(y_1 - y_0) + y'_0 + y'_1,$$

$$\beta = 3(y_1 - y_0) - 2y'_0 - y'_1,$$

$$\gamma = y'_0,$$

$$\delta = y_0,$$

Finally, it is worth mentioning that the derivatives x'_0, x'_1, y'_0, y'_1 are actually not specified themselves, but rather only their ratios are:

$$\frac{y'_0}{x'_0} = \left.\frac{dy}{dx}\right|_{P_n} = \tan\theta_n \Rightarrow y'_0 = (\tan\theta_n)x'_0 \quad \forall x'_0, x'_1, \tag{31}$$

$$\frac{y'_1}{x'_1} = \left.\frac{dy}{dx}\right|_{P_0} = 0 \Rightarrow y'_1 = 0 \quad \forall x'_0, x'_1. \tag{32}$$

This means that the equations (29) and (30) define a family of ∞^2 curves for all the possible values of (x'_0, x'_1). The choice of these two parameters can be made by optimizing on some additional performance index. Specifically, it may be useful to find an optimal tradeoff between maximal curvature of the path and its length.

To illustrate why this could be the case, consider Figure 6 where two paths are shown corresponding to different choices of (x'_0, x'_1). Both paths satisfy the boundary conditions $P_0 = (10\,\text{m},\ 0\,\text{m})$, $P_1 = (1\,\text{m},\ 0\,\text{m})$, $(\mathrm{d}y/\mathrm{d}x)_0 = 1$, $(\mathrm{d}y/\mathrm{d}x)_1 = -1$. The solid line path corresponds to $(x'_1, x'_0) = (1, 1)$, and shows a maximum curvature of about 32.9 rad/m, while the dashed line path corresponds to $(x'_1, x'_0) = (3, 3)$, and has a maximum curvature of 6.8 rad/m at the expense of a larger length. Even if the mobile robot used in this research is a differential drive one (and can thus drive infinite curvature paths), it may be indeed useful to design paths having bounded curvature. In particular, the parameters (x'_1, x'_0) may be selected by (numerically) optimizing a suitable performance index $\mathcal{J}$ taking into account the maximum path curvature and its length:

$$(x'_1, x'_0) = \arg\min_{x'_1, x'_0} \mathcal{J} : \mathcal{J} = \lambda \int_0^1 \sqrt{(x'^2(\xi) + y'^2(\xi))}\,\mathrm{d}\xi + \max_{\xi} |\kappa(\xi)|, \qquad (33)$$

where $x'(\xi), y'(\xi)$ are the derivatives with respect to ξ of the curve components given in equations (29) and (30), and κ is the curvature of the same curve. The parameter λ represents the relative weight of length over maximum curvature within the performance index $\mathcal{J}$: if $\lambda \to 0$, the length of the resulting path may tend to infinity, while if $\lambda \to \infty$, the resulting path tends to a straight path, eventually having pointwise infinitely large curvature (turning on the spot) on the boundary points in order to meet the orientation boundary conditions. An example of the obtained results is shown in Figure 7 where three paths relative to the same boundary conditions $(x_1, y_1, (\mathrm{d}y/\mathrm{d}x)_1, \kappa_1) = (0, 0, 0, 0)$, $(x_0, y_0, (\mathrm{d}y/\mathrm{d}x)_0, \kappa_0) = (5, 5, 0, 0)$, but different values of λ ($\lambda = 10,\ 1,\ 0.1$) are plotted. The bottom plot in Figure 7 clearly shows that the smaller values of maximal curvature are obtained at the expense of longer paths. The maximization of $\mathcal{J}$ has been performed numerically with a Nelder-Mead type simplex search method provided in the Matlab® software.

Figure 6 Two spline-paths obtained from different values of (x'_1, x'_0)

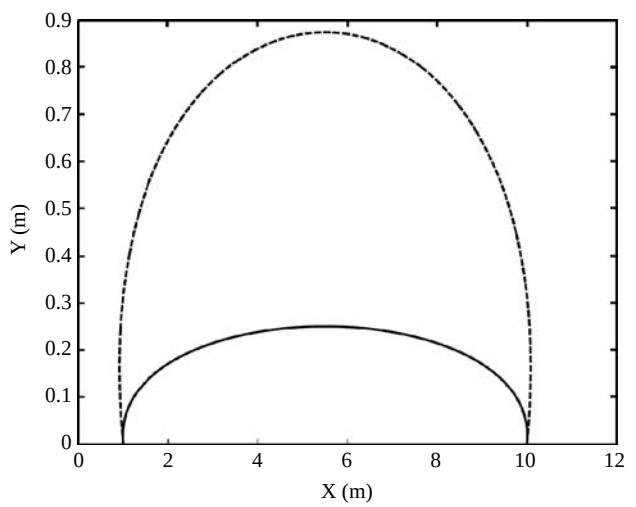

Figure 7 Path-planning examples: the star, diamond, and square points correspond to $\lambda = 10$, 1, 0.1, respectively, i.e. solid, dotted, and dashed paths in the upper plot

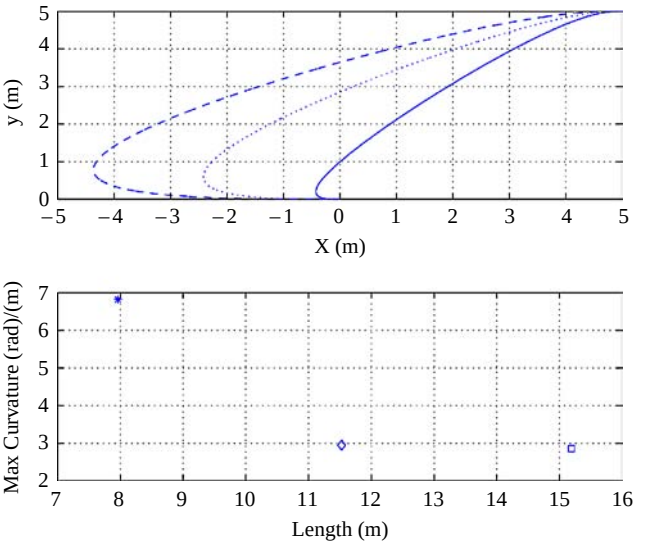

Finally, note that the last driven point P_n is always chosen at a small distance from the starting point P_0 (typically less than 1 m) with no obstacle in the way. If a sudden obstruction stands in the way, the vehicle stops using its proximity sensors until the way is clear again.

4.2 The automated olfactory inspection

Once that the inspection path Γ_R has been defined by joining the learned and returning portions, the vehicle is ready to perform its task of automated olfactory monitoring. During this step, the operator serves as a remote supervisor analyzing sensory data and images via wireless communication with the robot. In order to gain robustness to external disturbances, the path tracking is not done in open loop by simply "playing back" the linear and angular velocities associated with the reference path Γ_R, but rather by implementing a nonlinear feedback control. Specifically, the trajectory tracking control law of Canudas de Wit *et al.* (1993) for the unicycle model is employed. The required pose estimate to close the loop is computed based on the trackball odometry, while feedforward reference velocity signals are taken from the log file of the reference inspection trajectory Γ_R. Figure 8 shows the path followed by the vehicle as estimated by its odometric system during an experiment using the trajectory tracking control. The cusps that are visible at approximately $(x, y) = (5\,\text{cm}, 0\,\text{cm})$ and $(x, y) = (28\,\text{cm}, 0\,\text{cm})$, are due to the reaction of the closed loop law to an external disturbance (strong manual push!).

5. Experimental results

In this section, experimental results are presented aimed at validating our approach for odour source detection. In order to simulate odour leakages in a laboratory environment, we used 50 cm high turrets with an ethanol beaker and a 10 cm diameter plastic bowl on the top (Figure 3(a)). The ethanol

Figure 8 Path followed by the vehicle using tracking control in a typical experiment

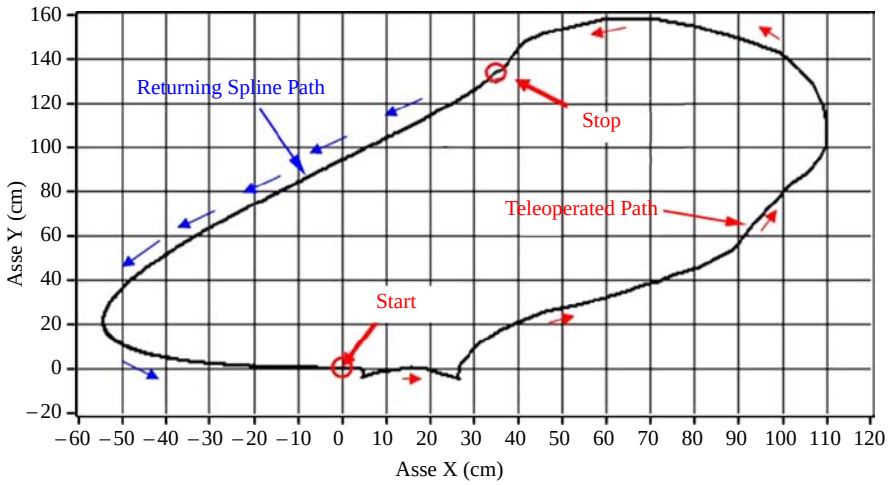

dripped into the bowl through a hole in the beaker at a rate of approximately 50 ml/h. Ethanol was used because it is not toxic, easy available, and easily detectable by the oxide sensors. First, the dynamic response of the mobile nose is studied, then a set of experiments was performed assessing the effectiveness and performance of the whole system.

5.1 Dynamic response

The mobile nose was subjected to a step stimulus by driving the robot at its nominal speed of 5 cm/sec along a 3 m straight path with an odour source placed exactly halfway. As suggested in Lilienthal and Duckett (2003), the sensor can be modeled as a first-order system and its dynamic response $r(t)$ to a step input as an exponential rise and decay:

$$r(t) = \begin{cases} r_1(t) & t < t_s \\ r_2(t) & t_s < t < t_s + \Delta t \\ r_3(t) & t_s + \Delta t < t \end{cases}, \tag{34}$$

$$r_1(t) = R_0, \tag{35}$$

$$r_2(t) = R_0 + (R_{max} - R_0)\left(1 - \exp\left(\frac{-(t - t_s)}{\tau_r}\right)\right), \tag{36}$$

$$r_3(t) = R'_0 + (R^*_{max} - R'_0)\left(\exp\left(\frac{-(t - t_s - \Delta t)}{\tau_d}\right)\right), \tag{37}$$

$$R^*_{max} = R_0 + (R_{max} - R_0)\left(1 - \exp\left(\frac{-\Delta t}{\tau_r}\right)\right), \tag{38}$$

where R_0 and R'_0 are the response level before and after the stimulus, R_{max} the saturation level, τ_r and τ_d the rise and decay time, respectively, and Δt is the rising interval. This set of parameters can be determined by fitting the model to experimental data using, for example, the Marquardt-Levenberg algorithm (Press *et al.*, 1997). A total of 1,200 data points, obtained from ten repeated trials, was used giving the results collected in Table I, expressed in terms of average value and standard deviation. Figure 9 shows the result of a typical run, instead. The black points refer to the gas sensor readings, whereas the solid black line is the fitted model. The sensor provides a slow response of about 1.5 s and an even longer recovery time of about 4.20. The duration of the stimulus depends on the vehicle's speed; however, its value does not affect significantly τ_r and τ_d.

Table I Model parameters obtained by fitting the sensor model with experimental data

Parameter (s)	Value
τ_r	1.50 ± 0.36
τ_d	4.20 ± 0.81
Δt	5.5 ± 1.10

Figure 9 Dynamic model of the olfactory sensor fitted to experimental data

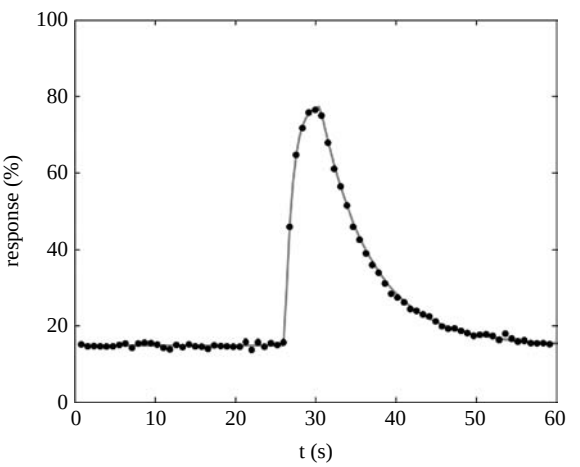

Notes: Grey continuous line: Sensor model. Black dots: Sensory data. Note that each dot represents the average value in a 1-second measuring window, being the sampling rate of the sensor 250 ms

5.2 Leakage detection

In order to test the effectiveness of our system in localizing odour sources along the inspection path, a set of experiments was performed in a 5 × 10 m weakly ventilated laboratory environment. Several odour sources were randomly spread along the path simulating fictitious leakages.

In a typical test, first, the inspection path was set by remotely driving the robot trough some points of interests. In a real industrial scenario, these points are potential leakage sites, such as valves, pressure vessels, tanks, pipes, etc. Next, the robot performed its automatic olfactory monitoring task while the number and position of the odour sources was changed along the inspection path. Figure 10 shows the results obtained from the mobile nose, expressed in terms of what we call the odour map of the path, for a test with five ethanol-leaking turrets. In the *x*-*y* plane, it is shown the path followed by the vehicle as estimated by the odometric system, whereas along the *z*-axis it is displayed the percentage relative resistance variation of the gas sensor in absolute value. The "ground truth" positions of the odour sources are indicated with black cross marks. The minimum relative distance between the turrets was 100 cm between the first and second source denoted with S_1 and S_2, respectively, in Figure 10. The mobile robot detected correctly all the odour sources. Table II lists for each of the source position $S_i = [S_{x,i}, S_{y,i}]$ the localization error E_i defined as:

$$E_i \frac{\sqrt{(S_{x,i} - M_{x,i})^2 + (S_{y,i} - M_{y,i})^2}}{\sqrt{S_{x,i}^2 - M_{y,i}^2}}, \qquad (39)$$

where $M_i = [M_{x,i}, M_{y,i}]$ is the location of the source i estimated by the olfactory system corresponding to the resistance variation peak.

The odour sources were located with an average error within 4.5 percent and a worst-case measurement of 5.7 percent. Note that E_i accounts also for errors due to the inaccuracy of the control and position estimation system.

The travel speed of the vehicle during this test was 5 cm/s. Other velocities of 15 and 25 cm/s were also analyzed but no significant difference in performance was observed.

A second experiment was performed using only two leaking turrets placed at a relative distance of about 60 cm in order to test the ability of the system to differentiate between two odour sources very close to each other. The odour map for this test is shown in Figure 11; the olfactory sensor successfully detected two distinct odour sources with an average error of 3.8 percent.

Figure 10 Odour map for a five-odour source inspection path

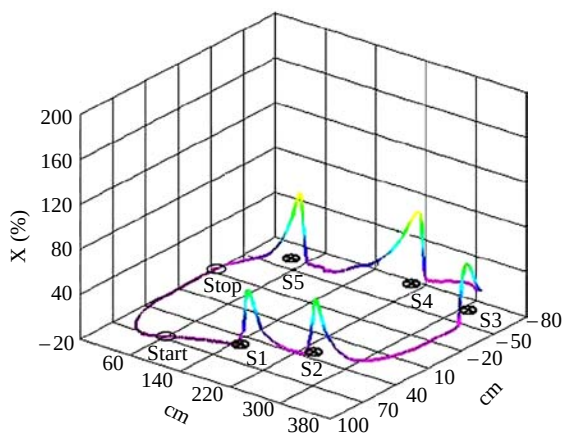

Table II Odour source localization errors for the five-source experiment shown in Figure 10

Source	S_1	S_2	S_3	S_4	S_5
E_i[%]	4.1	4.2	3.8	4.6	5.7

Figure 11 Odour map for an inspection path with two odour sources 60 cm close to each other

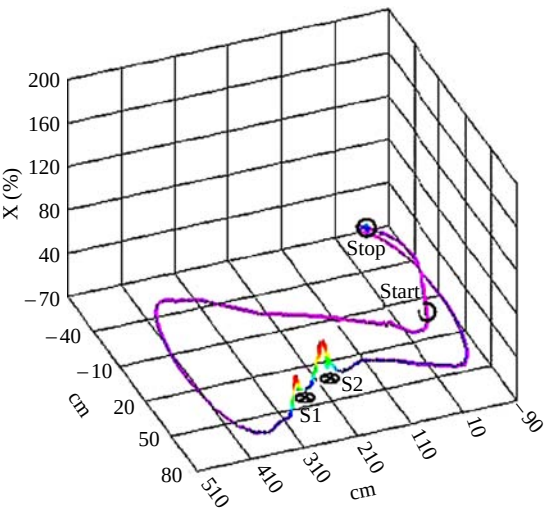

6. Conclusions

A mobile robotics application was described aiming at the development of an electronic sentry for automated olfactory inspection of hazardous industrial environments. A smart olfactory system sensor was presented and integrated with a differential drive vehicle providing the ability to build real-time odour maps along a prerecorded path. The envisaged strategy for automated inspection was described based on standard nonlinear feedback control approach for trajectory tracking, and a novel path planning solution for the optimal tradeoff between polynomial spline length and maximal (absolute) curvature along the path. The olfactory system showed to be effective in preliminary experimental trials to locate multiple odour sources and it could be employed in intelligent monitoring of chemical warehouses and industrial sites against hazardous gas leakages, thus resulting in an increase in the safety level for human operators. Future work will focus on multirobot olfaction applications, which may benefit from the PnP communication interface, and on integrating an obstacle avoidance strategy within the guidance control.

References

Borenstein, J. and Feng, L. (1996), "Measurement and correction of systematic odometry errors in mobile robots", *IEEE Journal of Robotics and Automation*, Vol. 12, pp. 869-80.

Canudas de Wit, C., Khennouf, H., Samson, C. and Sordalen, O.J. (1993), "Non linear control design for mobile robots", *Recent Trends in Mobile Robots*, World Scientific Pub. Co. Inc., Hackensack, NJ, pp. 121-30.

IEEE Std. 1451.2 (1997), *Standard for a Smart Transducer Interface for Sensors and Actuators – Transducer to Microprocessor Communication Protocols and Transducer Electronic Data Sheet (TEDS) Formats*, The Institute of Electrical and Electronics Engineers, Inc., New York, NY.

Ishida, H., Suetsugu, K., Nakamoto, T. and Moriizumi, T. (1994), "Study of autonomous mobile sensing system for localization of odour source using gas sensors and anemometric sensors", *Sensors and Actuators*, Vol. 45, pp. 153-7.

Kleperis, J., Lusis, A., Zubkans, J. and Veidemanis, M. (1999), "Two years' experience with Nordic e-nose", *Proc. Int. Sym. on Olfaction and Electronic Nose, Technical University, Graz, May 31-June 2*, pp. 11-14.

Lee, K. (2000), "IEEE 1451: a standard in support of smart transducer networking", *Proc. IEEE Instrumentation and Measurement Technology Conference, Baltimore, MD, USA*, pp. 525-8.

Lilienthal, A. and Duckett, T. (2003), "A stereo electronic nose for a mobile inspection robot", *Proc. of the IEEE International Workshop on Robotic Sensing, Orebro, Sweden*, June 5-6.

Lilienthal, A., Wandel, M., Weimar, U. and Zell, A. (2001), "Sensing odour sources in indoor environments without a constant airflow by a mobile robot", *Proc. of IEEE International Conf. on Robotics and Automation, Seoul, South Korea*, May 21-26, pp. 4005-10.

Marques, L. and de Almeida, A.T. (2000), "Electronic nose-based odour source localization", *Proc. of 6th International Workshop on Advanced Motion Control, Nagoya, Japan*, March 30-April 1, pp. 36-40.

Nakamoto, T., Ishida, H. and Moriizumi, T. (1999), "A sensing system for odour plumes", *Analytical Chem. News and Features*, Vol. 1, pp. 531-7.

Olafsson, R., Martinsdottir, E., Olafsdottir, G., Sigfusson, S.I. and Gardner, J.W. (1992), "Monitoring of fish freshness using tin oxide sensors", in Gardner, J. and Bartlett, P.N. (Eds), *Sensors and Sensory Systems for an Electronic Nose*, Kluwer, Dordrecht, pp. 257-72.

Persaud, K.C. and Dodd, G. (1982), "Analysis of discrimination mechanisms in the mammalian olfactory system using a model nose", *Nature*, Vol. 299, pp. 352-5.

Persaud, K.C., Pisanelli, A.M., Szyszko, S., Reichl, M., Horner, G., Rakow, W., Keding, H.J. and Wessels, H. (1999), "A smart sensor for monitoring environmental changes in closed systems: results from the MIR space station", *Sensors and Actuators B: Chemical*, Vol. 55 Nos 1/2, pp. 118-26.

Press, W.H., Teukolsky, S.A., Vettering, W.T. and Flannery, B.P. (1997), *Numerical Recipes in C*, Chapter 7, Cambridge University Press, Cambridge.

Russell, R.A. (2001), "Survey of robotic applications for odour-sensing technology", *The International Journal of Robotic Research*, Vol. 20 No. 2, pp. 144-62.

Russell, R., Thiel, D. and Mackay-Sim, A. (1995), "Sensing odour trails for mobile robot navigation", *Proc. IEEE International Conference on Robotics and Automation, Nagoya, Aichi, Japan*, May 21-27, pp. 2672-7.

Ryan, M., Zhou, H., Buehler, M., Manatt, K., Mowrey, V., Jackson, S., Kisor, A., Shevade, A. and Homer, M. (2004), "Monitoring space shuttle air quality using the jet propulsion laboratory electronic nose", *IEEE Sensors Journal*, Vol. 4 No. 3, pp. 337-47.

Stella, E., Musio, F., Vasanelli, L. and Distante, A. (1995), "Goal-oriented mobile robot navigation using an odour sensor", *Proc. of the Intelligent Vehicles Symposium*, pp. 147-51.

Taurino, A.M., Distante, C., Siciliano, P. and Vasanelli, L. (2003), "Quantitative and qualitative analysis of VOCs mixtures by means of a microsensors array and different evaluation methods", *Sensors and Actuators B: Chemical*, Vol. 93 Nos 1/3, pp. 117-25.

Watson, J. (1984), "The tin oxide gas sensor and its applications", *Sensors and Actuators*, Vol. 5, pp. 29-42.

Winquist, F., Hornsten, E.G., Sundgren, H. and Lundstrom, I. (1993), "Performance of an electronic nose for quality estimation of ground meat", *Measurement Science and Technology*, Vol. 4, pp. 1493-500.

Further reading

Brockett, R. (1983), "Asymptotic stability and feedback stabilization", in Brockett, R.W., Millmann, R.S. and Sussmann, H.J. (Eds), *Stabilization in Differential Geometric Control Theory*, Birkhauser, Boston, MA, pp. 181-91.

Corresponding author

Giulio Reina can be contacted at: giulio.reina@unile.it

To purchase reprints of this article please e-mail: **reprints@emeraldinsight.com**
Or visit our web site for further details: **www.emeraldinsight.com/reprints**